DOI 10.1007/s11029-018-9734-8
Mechanics of Composite Materials, Vol. 54, No. 2, May, 2018 (Russian Original Vol. 54, No. 2, March-April, 2018)

NONLINEAR DEFORMATION OF A PIECEWISE HOMOGENEOUS CYLINDER UNDER THE ACTION OF ROTATION

V. M. Akhundov,[*] and M. M. Kostrova

Keywords: *piecewise homogeneous cylinder, square fiber, free rotation, centrifugal force, large displacements and deformations, finite-difference method*

Deformation of a piecewise cylinder under the action of rotation is investigated. The cylinder consists of an elastic matrix with circular fibers of square cross section made of a more rigid elastic material and arranged doubly periodically in the cylinder. Behavior of the cylinder under large displacements and deformations is examined using the equations of a nonlinear elasticity theory for cylinder constituents. The problem posed is solved by the finite-difference method using the method of continuation with respect to the rotational speed of the cylinder.

Introduction

The deformation of round cylinders of homogeneous materials rotating around their symmetry axis has been investigated in detail in the linear mechanics of deformation, and the corresponding bibliography adequately enough is presented in [1]. In [2], inertial energy stores (flywheels) made of rigid composite materials are considered. In [3], with the help of equations of the linear elasticity theory, the problem on stresses in a rotating cylindrical orthotropic pipe is solved. Results are presented at free and rigid fits of the pipe for the cases of its axial and circular reinforcing. In [4], the redistribution of stresses in a disk with an elastomeric matrix in conditions of stress relaxation during creep of the matrix is considered. The problem is solved in a vectorially and physically linear statement. In [5, 6], plane strain and plane stress

National Metallurgical Academy of Ukraine, Dnepropetrovsk, Ukraine
[*]Corresponding author; e-mail: akhundov@ua.fm

Translated from Mekhanika Kompozitnykh Materialov, Vol. 54, No. 2, pp. 345-360 , March-April, 2018. Original article submitted June 22, 2017.

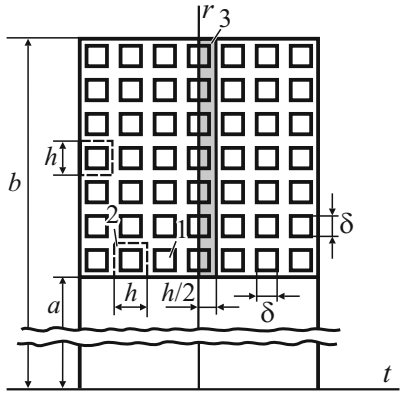

Fig. 1. Axial section of the cylinder in its initial state: 1 — fiber of square cross section; 2 — annular element; 3 — half of disk layer to the right of the central section.

states of a cylindrical flywheel with initial stresses caused by the circular winding of fibers and of matrix are investigated. The state of rotating elastoplastic disks is described in [7, 8]. In [8], a solution of the problem on the secondary creep of a rotating disk is also given. The problem on the elastoplastic behavior of a disk at a power-law hardening of its material is solved in [9]. In [10], a rotating disk is calculated according to experimental tensile diagrams of its material, without their simplifying schematization, by the method of variable elastic parameters.

Large inertia-caused deformations of rotating cylinders were found to be investigated only in [11-13]. In [11], problems in the plane statement for homogeneous cylinders and cylinders poorly reinforced with fibers in axial, circular, and radial directions were solved. The investigations were carried out using the applied theory of fibrous media [14] based on a material model where the macroscopic stresses are determined by additive contributions of matrix stresses and axial tension or constrained compression forces of fibers. In [12], employing the applied theory, the axisymmetric deformation of cylinders with fibers in circular and radial directions at different fits on the internal boundary surface were considered.

In [13], on the basis of single-level applied and two-level carcass theories, problems cylinders with two- and three-orthogonal reinforcement schemes were solved. The carcass theory [15] includes the macromechanical level, at which the macrovalue-boundary problem is solved for a body as a whole. At the a micromechanical level, for the central blocks of representation of the reinforced material of a body, microboundary-value problems were solved using the model of a piecewise homogeneous medium and conditions from the macromechanical level in the iterative procedure considering the interaction of the levels of analysis.

The model of a piecewise homogeneous medium methodologicalally most precisely reflects the behavior of a body of fibrous structure. In the given approach, the a matrix and fibers are considered as contacting interacting bodies on the basis of equations of the mechanics of deformable solids (MDS) for the matrix and each of reinforcing fibers. But, because of the limitated computing resources, the model of a piecewise homogeneous medium in a “pure” form can be used only for a small number of bodies with a unidirectional reinforcement in particular loadings. As such an object, we investigated a rotating cylinder whose elastic matrix was reinforced with circular fibers of square section of a more rigid elastic material.

1. Statement of the problem

The problem on deformation of an elastic cylinder consisting of a matrix and circular fibers under the action inertia forces caused by rotation of the cylinder around its symmetry axis is solved. Fibers of square section are arranged in the matrix of the cylinder doubly periodically with identical periods in the axial and radial directions. The cylinder was modeled as an

assembly of annular elements of square cross section made of the matrix material and containing fibers of square section as a reinforcement.

On Fig. 1, the axial section of a nondeformed cylinder with a internal radius $r = a$ and external radius $r = b$ is shown. The cylinder includes cylindrical layers of identical thickness h reinforced with circular fibers of identical square cross section with sides δ. The cylinder was also considered as set of disk layers of thickness h with one circular fiber in each layer (square packing).

The axisymmetric deformation of the cylinder corresponding to the macroscopically plane strain state where the length of the cylinder remained constant was considered. In view of symmetry of the problem, the problem was solved for half of disc layer of thickness $h/2$. Such a layer is enclosed between two cross sections of the cylinder one of which passes through axial lines of fibers and another — through the matrix between fibers. The distance between the sections is equal to half of the period of reinforcing in the axial direction.

A Lagrangian system of cylindrical coordinates $\hat{\theta}^1$, $\hat{\theta}^2$, $\hat{\theta}^3$ was used, where $\hat{\theta}^1$, $\hat{\theta}^2$, and $\hat{\theta}^3$ are the axial, circular, and radial coordinates, respectively. In the reference configurations of the cylinder, the coordinates were designed as $t, \varphi,$ and r, respectively. The axial coordinate t was measured from the central section, passing through the axial lines of fibers in a disk layer. Along with the radial coordinate r, the thickness coordinate $z = r - a$ measured from the internal surface of the cylinder was used. The physical components of vectors and tensors in the reference system of coordinates are labelled with coordinate indices in parentheses.

The quantities related to the matrix and fibers are marked by the subscript $n = 0,1,2,...,n_{\max}$; the value $n = 0$ corresponds to the matrix, but $n = 1, 2,...,n_{\max}$ specify nanofibers and the annular elements including fibers numbered in the direction from an internal surface of the cylinder to the external one; $n_{\max}$ is the number of fibers and annular elements in the part of the cylinder for which the boundary-value problem is solved. The quantities without a subsript n are related to the matrix and each fiber or to the cylinder as a whole.

2. Equations of the problem

Let us start from the general equations of nonlinear mechanics determining tensor components of the Cauchy–Green measure of deformation [16]. For the components of axisymmetric deformations of the matrix and fibers in the cylinder, we have relations determining them as functions of the axial and radial coordinates, *t* and *r*:

$$g_{n(11)} = \lambda_{n1}^2 = \left(1 + \frac{\partial u_{n(1)}}{\partial t}\right)^2 + \left(\frac{\partial u_{n(3)}}{\partial t}\right)^2,$$

$$g_{n(22)} = \lambda_{n2}^2 = \left(1 + \frac{u_{n(3)}}{r}\right)^2, \tag{2.1}$$

$$g_{n(33)} = \lambda_{n3}^2 = \left(1 + \frac{\partial u_{n(3)}}{\partial r}\right)^2 + \left(\frac{\partial u_{n(1)}}{\partial r}\right)^2,$$

$$g_{n(13)} = \lambda_{n1}\lambda_{n3}\cos\omega_{n13} = \frac{\partial u_{n(1)}}{\partial r} + \frac{\partial u_{n(3)}}{\partial t} + \frac{\partial u_{n(1)}}{\partial t}\frac{\partial u_{n(1)}}{\partial r} + \frac{\partial u_{n(3)}}{\partial t}\frac{\partial u_{n(3)}}{\partial r},$$

$$n = 0,1,...,n_{\max},$$

where λ_{n1}, λ_{n2}, and λ_{n3} are stretch ratios in directions of the coordinate lines $\hat{\theta}^1$, $\hat{\theta}^2$, and $\hat{\theta}^3$ (t, φ, r), respectively; ω_{n13} is the coordinate angle between the $\hat{\theta}^1$ and $\hat{\theta}^3$ coordinate lines (the components of vectors and tensors equal to zero owing to symmetry of the problem considered are not presented).

In the case of compressible materials of the matrix and fibers, components of their stress and strain tensors are connected by the relations [17]

$$J\sigma_{n(ij)} = 2\sum_{p} \frac{\partial W_n}{\partial I_{np}} \cdot \frac{\partial I_{np}}{\partial g_{n(ij)}},\ i, j = 1,\ldots, 3,\ n = 0,1,...,n_{\max}, \tag{2.2}$$

where $W_n = W_n[I_{n1}(g_{n(ij)}),\ I_{n2}(g_{n(ij)}),...,I_{nq}(g_{n(ij)})]$ is the elastic potential of the matrix ($n = 0$) or fibers ($n = 1,\ 2,...,n_{\max}$) material, which depends on the invariants $I_{n1}, I_{n2},...,I_{nq}$ of its strain tensor.

Employing the general equilibrium equations of MDS at large deformations [18], the following equilibrium equations for the axisymmetrically deforming cylinder in the metric of reference configuration were obtained:

$$\begin{gathered}\frac{\partial t_{n(11)}}{\partial t} r + \frac{\partial t_{n(31)}}{\partial r} r + t_{n(31)} = 0, \\ \frac{\partial t_{n(13)}}{\partial t} r + \frac{\partial t_{n(33)}}{\partial r} r + t_{n(33)} - t_{n(22)} + \rho_n r F_{n(3)} = 0,\ n = 0,1,...,n_{\max}.\end{gathered} \tag{2.3}$$

Here, $t_{n(ij)}$ are the physical components of the asymmetric Piola–Kirchhoff stress tensor of the matrix and fibers of the cylinder, of which different from zero are the following ones:

$$\begin{gathered}t_{n(11)} = J_n \sigma_{n(11)} \left(1 + \frac{\partial u_{n(1)}}{\partial t}\right) + J_n \sigma_{n(13)} \frac{\partial u_{n(1)}}{\partial r}, \\ t_{n(13)} = J_n \sigma_{n(13)} \left(1 + \frac{\partial u_{n(3)}}{\partial r}\right) + J_n \sigma_{n(11)} \frac{\partial u_{n(3)}}{\partial t}, \\ t_{n(31)} = J_n \sigma_{n(31)} \left(1 + \frac{\partial u_{n(1)}}{\partial t}\right) + J_n \sigma_{n(33)} \frac{\partial u_{n(1)}}{\partial r},\end{gathered} \tag{2.4}$$

$$\begin{gathered}t_{n(33)} = J_n \sigma_{n(33)} \left(1 + \frac{\partial u_{n(3)}}{\partial r}\right) + J_n \sigma_{n(31)} \frac{\partial u_{n(3)}}{\partial t},\ n = 0,1,...,n_{\max}; \\ t_{n(22)} = J_n \sigma_{n(22)} \left(1 + \frac{u_{n(3)}}{r}\right),\ n = 0,1,...,n_{\max}.\end{gathered} \tag{2.5}$$

The distinctive features of a rotating cylinder with elastic constituents is the action of centrifugal forces on its matrix and fibers and varying distances from their material points to the cylinder axis. In Eqs. (2.3), the radial component of density of the mass forces acting on components of the rotating cylinder is

$$F_{n(3)} = (r + u_{n(3)})\omega^2,\ n = 0,1,...,n_{\max},$$

where $\omega = 2\pi f$ is the angular speed of rotation; f is the number of revolutions per second.

Components of the symmetric Piola–Kirchhoff tensor $J\sigma_{(ij)}$ can be expressed in terms of the components p_{ij} of stress vectors on the $\hat{\theta}^i$ -coordinate surfaces related to the normalized vector basis of coordinate system in the deformed configuration of the cylinder [19]:

$$\begin{gathered}J\sigma_{(11)} = \lambda_1^{-1}\lambda_2\lambda_3 \sin\omega_{23} p_{11}\ J\sigma_{(22)} = \lambda_2^{-1}\lambda_1\lambda_3 \sin\omega_{13} p_{22}, \\ J\sigma_{(33)} = \lambda_3^{-1}\lambda_1\lambda_2 \sin\omega_{12} p_{33},\ J\sigma_{(13)} = \lambda_2 \sin\omega_{23} p_{13}\end{gathered} \tag{2.6}$$

(the subscript *n* has been omitted here).

3. Construction of a numerical solution of the problem

The geometrical (2.1), physical (2.2), and equilibrium (2.3) equations, together with Eqs. (2.4) and (2.5), were considered as resolving equations of the boundary-value problem for the piecewise homogeneous cylinder. The components $u_{n(1)}$ and $u_{n(3)}$ of displacement vectors and $t_{n(11)}$, $t_{n(13)}$, $t_{n(31)}$, and $t_{n(33)}$ of stress tensors in the matrix and fibers were assumed as the basic quantities. The strains $g_{n(11)}$, $g_{n(22)}$, and $g_{n(33)}$ and stresses $t_{n(22)}$ in the resolving equation were expressed in terms of the basic quantities with the help of Eqs. (2.1) and (2.5).

For each cylinder constituent, the boundary conditions at which the boundary-value problem was solved express the absence of axial displacements and transverse strains in the surfaces $t = 0$ and $t = h/2$:

$$u_{n(1)}\,|_{t=0} = 0\,,\quad g_{n(13)}\,|_{t=0} = 0\,,\quad u_{n(1)}\,|_{t=h/2} = 0\,,$$
$$g_{n(13)}\,|_{t=h/2} = 0\,,\quad n = 0,\,1,\,2,...,n_{\max}\,. \tag{3.1}$$

In the load-free internal and external surfaces of the cylinder, the components of the asymmetric Piola–Kirchhoff tensor were assumed equal to zero:

$$t_{n(3j)=0}\,|_{r=a} = 0,\qquad t_{n(3j)=0}\,|_{r=b} = 0\,,\ n = 0,\ j = 1,\,3\,. \tag{3.2}$$

The conditions of joint deformation were given proceeding from the equality of components of the vectors of displacements and stresses in the matrix and fiber interfaces. In these conditions, the quantities related to the matrix are labeled with the subscript *m*: in the cylindrical interface of matrix and an *n*th fiber,

$$u_{m(1)}(t,r) = u_{n(1)}(t,r)\,,\ u_{m(3)}(t,r) = u_{n(3)}(t,r)\,,$$
$$t_{m(31)}(t,r) = t_{n(31)}(t,r)\,,\ t_{m(33)}(t,r) = t_{n(33)}(t,r)\,, \tag{3.3}$$
$$0 \le t \le \delta/2\,,\ z = nh - (h+\delta)/2\,,\ z = nh - (h-\delta)/2\,,$$
$$m = 0\,,\ n = 1,\,2,...,n_{\max}\,.$$

In the transverse plane $t = \delta/2$ between an *n*th fiber and matrix

$$u_{m(1)}(t,r) = u_{n(1)}(t,r)\,,\quad u_{m(3)}(t,r) = u_{n(3)}(t,r)\,,$$
$$t_{m(11)}(t,r) = t_{n(11)}(t,r)\,,\quad t_{m(13)}(t,r) = t_{n(13)}(t,r)\,, \tag{3.4}$$
$$t = \delta/2\,,\ nh - (h+\delta)/2 \le z \le nh - (h-\delta)/2\,,\quad m = 0\,,\ n = 1,...,n_{\max}\,.$$

The derivatives of the first order of basic quantities with respect to the axial and radial coordinates t and r were approximated with the help of finite-difference relations of the second order of accuracy [20]. Together with boundary conditions (3.1) and (3.2) and conditions of joint deformation of the matrix and fibers (3.3) and (3.4), a system of the nonlinear equations in the basic quantities is formed at the central points of the two-dimensional area $0 \le t \le h/2$, $a \le r \le b$. This system of equations was solved using the discrete Newton's method [21]. The uniqueness of solution of the boundary-value problem was ensured by continuation of the solution relative to the angular rotation speed of the cylinder. As a result of solution of the boundary-value problem at finite angular speeds ω, with the use of Eq. (2.6), the nodal values of displacements $u_{n(i)}$, deformations λ_{ni} and ω_{nij} and stresses p_{nij} for the matrix ($n = 0$) and fibers ($n = 1,\,2,...,n_{\max}$) were found.

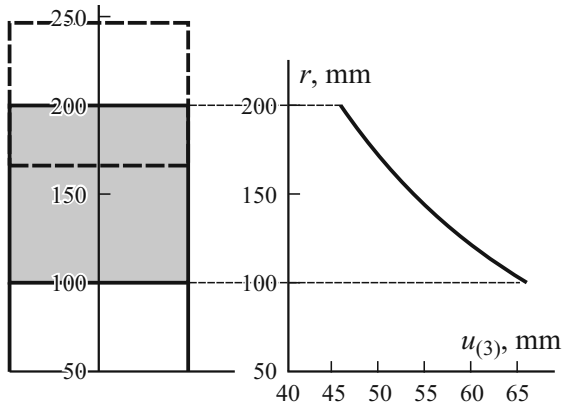

Fig. 2. Contour of axial section of the cylinder in the initial state (——) and in rotation with the speed $\omega = 2\pi \cdot 80$ s^{-1} (– – –) and the distribution of radial strains $u_{(3)}$ in cross sections of the cylinder.

4. Numerical results

The cylinder was considered as set of disk layers with 100 annular elements. The internal and external radii of the cylinder were $a = 100$ and $b = 200$ mm, respectively. The side of cross section of quadratic fibers was $\delta = 0.6h = 0.6$ mm, and the fibers were packed at distances between the axial lines of adjacent fibers $h = 1$ mm, with a fiber filling factor $k_f = \delta^2 / h^2 = 0.36$. The properties of the matrix and fibers were specified by the three-constant Levinson–Burgess and two-constant Bleitz potential [22], respectively. The elastic parameters of matrix were $E_m = 4$ MPa, $\nu_m = 0.46$, and $\beta_m = 1$ and of fibers — $E_f = 68$ MPa and $\nu_f = 0.4$. The densities of matrix and fiber materials were identical — $\rho_m = \rho_f = 1.1 \cdot 10^3$ kg/m^3.

Let us analyze solution results of the problem on the basis of the grid of nodal points of a finite-difference scheme with seven equidistant nodal points on sections of $0 \le t \le 0.3$ mm and $0.3 \le t \le 0.5$ mm, two of which coincide on interfaces. On intervals along the coordinate *r* in fibers and between them, also were seven nodal points (the coordinate lines corresponding to the given grid of nodal points are shown on Fig. 3).

Figure 2 shows contour lines of the cylinder in its initial state and at the angular speed $\omega = 2\pi \cdot 80$ s^{-1} and the graph of change on the radial displacements $u_{(3)}$ in cross sections of the cylinder in relation to the radial coordinate *r*. The generatrices of internal and external boundary surfaces of the deformed cylinder, within the limits of error of the image, are straight lines parallel to its axis. The radial displacements of the central section $t = 0$ changes from $u_{(3)} = 66.1$ mm at $r = a = 100$ mm to $u_{(3)} = 45.6$ mm at $r = b = 200$ mm. The internal and external radii in the deformed state become $a^* = a + u_{(3)}\,|_{t=0,r=a} = 166.1$ mm and $b^* = b + u_{(3)}\,|_{t=0,r=b} = 245.6$ mm, respectively. The cylinder thickness at the central section thus is $H^*\,|_{t=0} = b^* - a^* = 79.5$ mm, instead of the former $H = b - a = 100$ mm.

On Fig. 3, the configurations of axial sections for four half-units of the annular elements located in the cylinder to the right of the central section are shown. Each of them includes three concentrically located annular elements. The first unit is separated from the nondeformed cylinder; the configuration of its axial section does not depend on its location in the cylinder and is given for comparison with the deformed unit. Other units are separated from the deformed cylinder at $\omega = 2\pi \cdot 80$ s^{-1}. The second assembly includes the 1th, 2nd, and 3rd annular elements adjacent to the internal surface of the cylinder and is bounded by the surfaces $z = 0$ and $z = 3h$. The third unit is formed from the external half of the 49th element, 50th and 51st elements and from the internal half of the 52nd element and is located between the surfaces $z = 48.5h$ and $z = 51.5h$. The fourth unit includes the adjacent to the external surface of cylinder 98th, 99th, and 100th elements and is located between the surfaces $z = 97h$ and $z = 100h$.

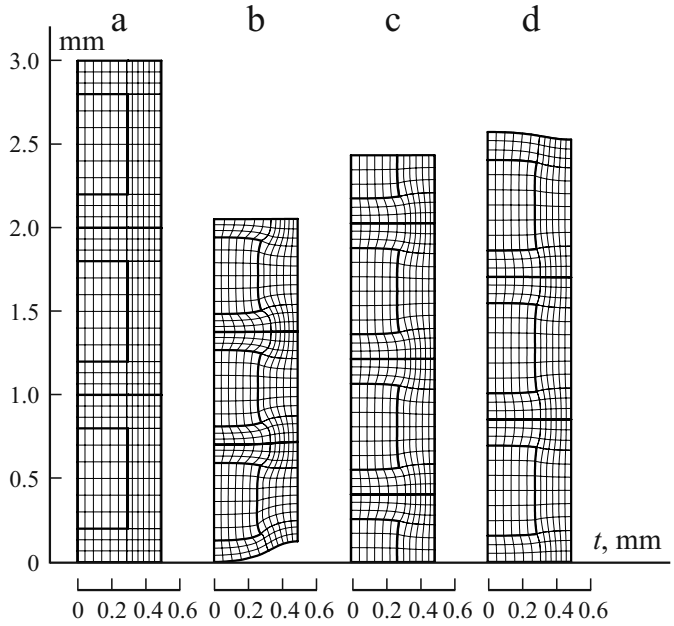

Fig. 3. Configurations of axial sections of units of ring elements of the cylinder: a — unit of three elements of the motionless cylinder; b, c, and d — units at rotation with $\omega = 2\pi \cdot 80$ s^{-1}, including the 1st, 2nd, and 3rd elements, half of the 49th, 50th, 51st, half of the 52nd element, and 98th, 99th, and 100th elements, respectively accordingly.

The configurations of axial sections of ring elements in the units are presented by grids of the coordinate lines $t = t_i$ and $z = z_i$ passing through the central points (t_i, z_i) of the finite-difference diagram used to solve the problem. They show how much more intensively deformed are the annular elements located closer to the internal surface of the cylinder.

Most strongly changes the configuration of the 1st element, whose internal surface is part of the boundary surface of the cylinder. The matrix near to the internal surface significantly moves inward the matrix layer $\delta / 2 \le t \le h / 2$ between fibers of the cylinder from the disk layer considered and the adjacent to it another disk layer. The bending deflection of internal surface of the cylinder was $f = 0.12$ mm (12% of the height $h = 1$ mm of cross section of the element in the nondeformed state). This effect is less expressed near the external surface of the cylinder, which also flexes inside the area occupied by the matrix, with a bending deflection $f = 0.05$ mm.

The deformed configurations of axial sections of the 1st and 2nd annular elements differ considerably between themselves. For the 2nd and 3rd elements, the distinction between their configurations is expressed less. As to the 3rd and 4th and subsequent pairs of adjacent elements, their configurations are close between themselves within the limits of representation error of the graphic material. This persists up to the pair of 98th and 99th elements inclusive. Only the configuration of the 99th element appreciablly differs from that of the 100th element. Thus, we come to the conclusion that the near-surface effect close to the internal surface of the cylinder penetrates at the depth of one or two periods of reinforcement by circular fibers, depending on the criterion used (this question will not be considered here), and close to its external surface, at the depth of one period of reinforcement.

On Fig. 4, the distributions of axial, circular, and radial stretch ratios λ_1, λ_2, and λ_3 and of the angular deformation ω_{13} along the generatrix of internal surface of the cylinder (of the first element) are illustrated. A characteristic feature is the axial lengthening on the section under fibers and shortening in the matrix layer. The curve of radial deformation λ_3 reflects a greater radial shortening under the fiber, where $\lambda_3 - 1 = -0.44$, and smaller in the matrix layer, at whose center $t = 0.5$ $\lambda_3 - 1 = -0.28$. The circular deformation λ_2 is practically constant, varying from $\lambda_2 = 1.661$ at $t = 0$ to $\lambda_2 = 1.662$ at $t = 0.5$; for the angular deformation, $\pi / 2 - \omega_{13} = 0$ at the free internal surface of the cylinder.

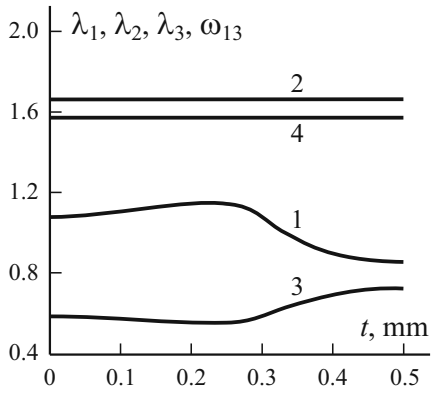

Fig. 4. Distributions of stretch ratios λ_1 (1), λ_2 (2), and λ_3 (3) and the coordinate angle ω_{13} (4) in the internal surface $z = 0$ of the 1st annular element of cylinder.

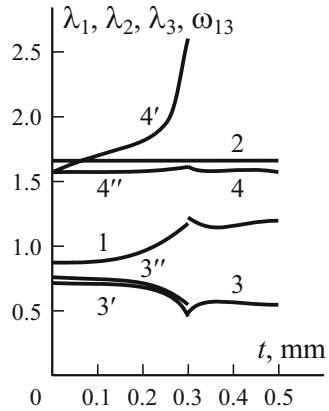

Fig. 5. The same in the internal surface $z = 0.2h$ of matrix and fiber in the 1st annular element of the cylinder. At a jump of a quantity in passing through the interface of constituents, the curves for the matrix and fibers are marked by numbers with one and two primes, respectively.

The distributions of deformation parameters along the generatrix of the cylindrical surface $z = (h-\delta)/2$, in which the "internal" interface between the first fiber with the matrix is located, are shown on Fig. 5. At the angular point $[\delta/2, (h-\delta)/2]$, the deformation parameters, except λ_2, are discontinuous. These discontinuities grow with degree of digitization of the problem, and the results diverge. The results for the angular point on the basis of the grid of nodal points used are formal to some extent by virtue of its singular character, as belonging to the line where the smoothness of contact surface of various materials is violated [23].

The gap of ω_{13} in the matrix material is $\omega_{13}|_{z=\to 0.3} - \omega_{13}|_{z=0.3\leftarrow} = 0.99$ (56.7°); in passing from the fiber to matrix, the gap is small (0.3°). The axial deformation λ_1 along the interface passes from shortenings near the central section to lengthenings near the matrix area and in the most matrix area of $0.3 \le t \le 0.5$ mm.

In going from the matrix to fiber, the radial λ_3 and angular ω_{13} deformations undergo a jump along all the interface. In the radial deformation, this jump arises owing to compression of the softer matrix by the more rigid fiber at their interaction.

The changes in deformation parameters along the generatrix of the median surface $z = 0.5$ mm of the first ring element are shown on Fig. 6. In going from the fiber to matrix, the functions λ_1 and ω_{13} undergo jumps: $\lambda_1 < 1$ within the limits of fiber and $\lambda_1 > 1$ in the matrix layer. The deformation λ_1 changes in the interval $0.84 \le \lambda_1 < 1.34$ jumpvise from the value $\lambda_1|_{\to 0.3} = 0.90$ on the left to $\lambda_1|_{0.3\leftarrow} = 1.04$ on the right. The angular deformation changes jumpvise from $\omega_{13}|_{\to 0.3} = 86.7°$ to

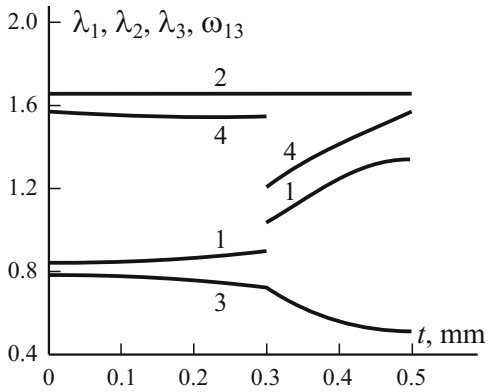

Fig. 6. Distributions of stretch ratios λ_1 (1), λ_2 (2), and λ_3 (3) and coordinate angle ω_{13} (4) in the median surface $z = 0.5h$ of the 1st annular element of cylinder.

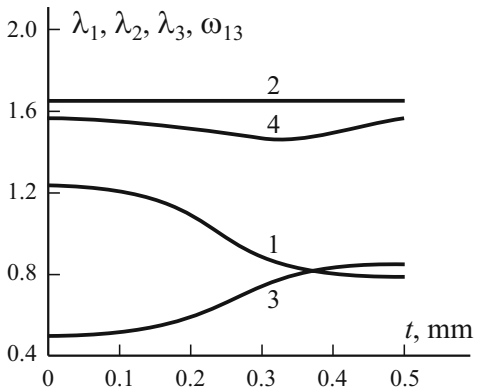

Fig. 7. The same in the surface $z = h$ of the 1st and 2nd annular elements of cylinder.

$\omega_{13}|_{0.3\leftarrow} = 69.1°$. The λ_3 curve undergoes a break in passing between cylinder components. The circular deformation λ_2 remains practically the same as at $z = 0$ everywhere in the element because of its small cross section $h \times h = 1 \times 1$ mm.

On Fig. 7, distributions of deformation in the surface $z = h$ separating the 1st and 2nd ring elements are illustrated. The axial deformation λ_1 decreases monotonically, changing from stretching ($\lambda_1 > 1$) in the zone between fibers to compression ($\lambda_1 < 1$) in the matrix layer $0.3 \le t \le 0.5$ mm. In fact, the displacement of binder from the region between adjacent fibers in the area of matrix layer (see also the configurations of units of annular elements on Fig. 3) is reflected here. The function λ_3 grows monotonically at the greatest values (in modulus) of shortening $\lambda_3 - 1 \cong -0.5$ at the center between fibers. The curve λ_2 is constant within the limits of error of its image. At the greatest shear deformation $\pi/2 - \omega_{13}$ near the place of passing to the matrix layer, the ω_{13} curve not much deviates from $\pi/2$.

On Fig. 8, distributions of the circular stress p_{22} in the central section $t = 0$ are depicted. They are shown on the intervals $0 \le z \le 3h$, $48.5h \le z \le 51.5h$, and $97h \le z \le 100h$ in the three units of ring elements illustrated on Figs. 3b, c, d. This stress undergoes jumps on interfaces between the matrix and fibers. In passing from one ring element to another located above it, this stress in the matrix and fibers decreases. In the matrix, the stress decreases from p_{22} =3.1 MPa in the internal surface $z = 0$ to p_{22} = 1.2 MPa in external surface $z = 100$ mm. In the median surface $z = 0.5h$ of the 1st fiber, p_{22} = 47.1 MPa, and in the median surface $z = 99.5h$ of the 100th fiber, p_{22} = 15.8 MPa. In passing from the matrix to fiber, this stress in the 1st element increases 22 and 17 times at the internal and external cylindrical interfaces 25 and 17 times, respectively, in the 100th element. In the elements near the median surface of the cylinder, in passing from the matrix to fiber, the stress increases 14 times in both the interfaces.

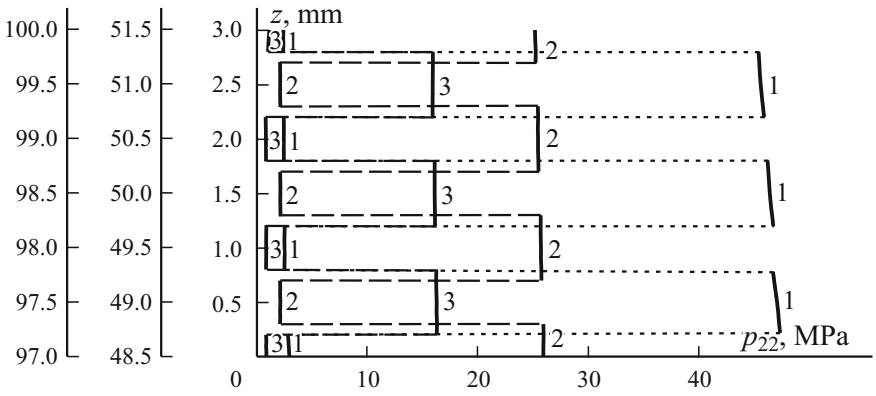

Fig. 8. Distributions of circular stresses p_{22} in the central section $t = 0$ on the intervals $0 \le z \le 3h$ (1), $48.5h \le z \le 51.5h$ (2), and $97h \le z \le 100h$ (3) of three units of annular elements of cylinder.

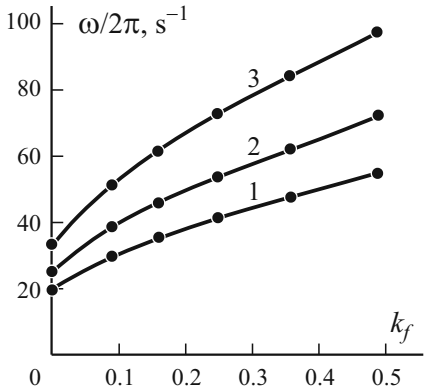

Fig. 9. Rotation speed $\omega / 2\pi$ as a function of fiber filling factor k_f, at displacements in the outer surface of cylinder $u_{(3)}$ = 10 (1), 20 (2), and 60 mm (3) and k_f = 0, 0.09, 0.16, 0.25, 0.36, and 0,49.

On Fig. 9, the rotation speed $\omega / 2\pi$ of cylinder as a function of fibers filling factor k_f is shown. The different curves correspond to rotations speeds at which the radial displacements $u_{(3)}$ in the external surface of the cylinder at the central section, and practically everywhere in this surface, are equal to 10, 20, and 60 mm. They are constructed using relations between the radial displacements in the external surfaces of cylinders with k_f = 0, 0.09, 0.16, 0.25, 0.36, and 0.49 and their rotation speeds. These filling factors correspond to square fibers with cross-sectional sides δ = 0, 0.3, 0.4, 0.5, 0.6, and 0.7 mm, respectively. The other parameters of cylinders and their reinforcement schemes were taken the same as at k_f = 0.36. The homogeneous cylinder was modeled using the general calculation algorithm and setting for fibers the same material properties as for the matrix. At the rotation speed $\omega = 2\pi \cdot 33.5$ s^{-1} of the homogeneous cylinder and $\omega = 2\pi \cdot 97.5$ s^{-1} of the cylinder with k_f = 0.49, their external radius was $a^* = a + 60$ mm. The thickness of cylinder wall changed from H^*=79 mm in the absence of fibers to H^*=75.5 mm at k_f = 0.49. In transition from the homogeneous cylinder to the cylinder with the specified fiber filling factor, the thickness of cylinder wall increased by one order of magnitude.

Conclusions

Based on the model of a piecewise homogeneous medium, investigated were the properties of an elastic cylinder reinforced periodically with circular fibers of square cross section in its macroscopically plane deformation during rotation

around its axial line. The pattern of deformations and stresses in the matrix and fibers of the cylinder at its rotation causing strong changes in its configuration was revealed. Established was the fact of displacement of matrix material from the areas between fibers in cylindrical layers in the field of disk layers occupied by the matrix. The near-surface effect was expressed in a considerably nonperiodic deformation of the ring elements of the cylinder adjacent to its internal and external surfaces. At a prescribed development of configuration of the cylinder, its rotation speed and stock of kinetic energy can be adjusted effectively by reinforcing it with circular fibers. The results obtained using the most detailed approach in MDS can help one to study the possibilities of axiomatic approaches in the mechanics of fibrous media as in [14, 15].

REFERENCES

1. K. Loffer, Die berechnung von Rotierenden Scheiben und Schalen, Göttingen, Springer, Verlag OHG (1961).
2. Composite materials: Handbook, eds. V. V. Vasil'ev and Yu. M. Tarnopolskii [in Russian], Mashinostroenie (1990).
3. M. Tervonen and A. Pramila, "Stresses in a hollow rotating cylindrically orthotropic tube," Mech. Compos. Mater., **32**, No. 6, P. 577-581 (1996).
4. G. G. Portnov and Ch. E. Bakis, "Estimation of limit strains in disk-type flywheels made of compliant elastomeric matrix composite undergoing radial creep," Mech. Compos. Mater., **36**, No. 1, 87-94 (2000).
5. G. Portnov, A. N. Uthe, I. Cruz, R. P. Fiffe, and F. Arias, "Design of steel-composite multirim cylindrical flywheels manufactured by winding with high tensioning and in situ curing. 1. Basic relations," Mech. Compos. Mater., **41**, No. 2, 139-152 (2005).
6. G. Portnov, A. N. Uthe, I. Cruz, R. P. Fiffe, and F. Arias, "Design of steel-composite multirim cylindrical flywheels manufactured by winding with high tensioning and in situ curing. 2. Numerical analysis," Mech. Compos. Mater., **41**, No. 3, 241-254 (2005).
7. U. Johnson and P. Mellor, Plasticity Theory for Engineers [Russian translation], M., Mashinostroenie (1979).
8. G. S. Pisarenko and N. S. Mozharovskii, Equations and Boundary-Value Problems of the Theory of Plasticity and Creep. Handbook [in Russian], Kiev, Nauk. Dumka (1981).
9. V. V. Sokolovsky, Plasticity Theory [in Russian], M., Vysh. Shkola (1969).
10. Thermal Strength of Mashine Parts, eds, I. A. Birger and B. F. Shora [in Russian], M., Mashnostroenie (1975).
11. V. M. Akhundov and T. A. Skripochka, "Large deformations of homogeneous and fiber-reinforced cylinders under the action of centrifugal forces," Mech. Compos. Mater.**, 45**, No. 3, 235-248 (2009).
12. V. M. Akhundov and T. A. Skripochka, "Axisymmetric deformation of revolving cylinders made of homogeneous and fiber-reinforced elastic materials," Mech. Compos. Mater., **47**, No. 2, 211-220 (2011).
13. V. M. Akhundov, "Modeling large deformations of fibrous bodies of revolution based on applied and carcass theories. 3. Rotational motion," Mech. Compos. Mater., **50**, No. 6, 809-816 (2014).
14. V. M. Akhundov, "Applied theory of composites with low fiber fillings at large deformations," Mekh. Kompos. Mater. Konstr., **7**, No. 1, 3-15 (2001).
15. V. M. Akhundov, "Carcass theory of fibrous media with uncurved and locally curved fibers at large deformations," Mech. Compos. Mater., **51**, No. 6, 683-694 (2015).
16. A. I. Lurye, Nonlinear Elasticity Theory [in Russian], M., Nauka (1980).
17. A. K. Malmeister, V. P., Tamuzh, and G. A. Teters, Strength of Polymer and Composite Materials [in Russian], Riga, Zinatne (1980).
18. Introduction into the Mechanics of Continuous Media, ed. K. F. Chernykh [in Russian], L., Izd. Leningr. Univ. (1984).
19. V. M. Akhundov, "Analysis of elastomeric composites based on fiber reinforced systems. 1. Development of design methods for composite materials," Mech. Compos. Mater., **34**, No. 6, 515-524 (1998).
20. G. A. Korn and T. M. Korn Mathematical Handbook for Scientists and Engineers: Definitions, Theorems and Formulas for Reference and Review, N.Y.: General Publ. Company (2000).

21. Dzh. Ortega and V. Reinboldt, Itegration Methods for Solving of Nonlinear Systems of Equations with Many Unknowns [Russian translation], M., Mir (1975).
22. K. F. Chernykh, Nonlinear Elasticity Theory in Machine-Building Calculations [in Russian], L., Mashinostroenie (1986).
23. V. Z. Parton, P. I. Perlin, Method of Mathematical Elasticity Theory[in Russian], M., Nauka (1981).